Increased early sodium current provokes familial atrial fibrillation and reduces effectiveness of sodium channel block

O'Reilly M[1*], Sommerfeld LC[1,2,3*], O'Shea C[1], Broadway-Stringer S[1], Andaleeb S[1], Reyat JS[1], Kabir SN[1], Malinova A[1], Delbue D[2,3], Fortmueller L[2,3], Gehmlich K[1,5], Pavlovic D[1], Skryabin BV[6], Holmes AP[1,7], Kirchhof P[1,3,4], Fabritz L[1,2,3,4]

[1]*Institute of Cardiovascular Sciences, University of Birmingham, UK*

[2]*University Center of Cardiovascular Science, University Heart and Vascular Center Hamburg, UKE Hamburg, Germany*

[3]*DZHK Standort Hamburg/Kiel/Luebeck, Germany*

[4]*Department of Cardiology, University Heart and Vascular Center UKE Hamburg, Germany*

[5]*Division of Cardiovascular Medicine, Radcliffe Department of Medicine and British Heart Foundation Centre of Research Excellence Oxford, University of Oxford, UK*

[6]*Medical Faculty, Core Facility Transgenic animal and genetic engineering Models (TRAM), University of Muenster, Germany*

[7]*Institute of Clinical Sciences, University of Birmingham, UK*

*equal contribution

Corresponding author:

Professor Larissa Fabritz

University Center of Cardiovascular Science

University Heart and Vascular Center, UKE Hamburg

Hamburg, Germany

E-Mail: l.fabritz@uke.de

1 Abstract

1.1 Aims

Atrial fibrillation (AF) is the most common cardiac arrhythmia. AF often develops due to concomitant cardiovascular conditions combined with a pre-existing atrial substrate. Familial, early onset forms of AF enable identification of this substrate. Pathogenic variants in genes encoding ion channels are associated with familial AF. The point mutation M1875T in the *SCN5A* gene, which encodes the α-subunit of the cardiac sodium channel $Na_v1.5$, has been associated with increased atrial excitability and familial AF. Designing a new murine model carrying the *Scn5a* -M1875T mutation enabled us to study this atrial substrate in detail.

1.2 Methods and Results

Left atrial cardiomyocytes from newly generated *Scn5a*-M1875T$^{+/-}$ mice showed a selective increase in the early (peak) cardiac sodium current, measured by patch clamp. Microelectrode recordings of intact left atria revealed larger action potential amplitudes and a faster peak upstroke velocity. Conduction was studied using optical mapping. When challenged with the sodium channel blocker flecainide, *Scn5a*-M1875T$^{+/-}$ left atria showed less conduction slowing than matched wildtype atria. *In vivo* analysis using electrocardiograms and echocardiography, as well as cardiac histology, excluded overt hypertrophy or heart failure in young adult mice.

1.3 Conclusion

The *Scn5a*-M1875T point mutation causes a cardiac sodium channel gain-of-function and suggests increased atrial peak sodium current as a potential trigger for increased atrial excitability and atrial fibrillation.

1.4 Translational Perspective

The observed changes highlight a selective increase in peak sodium current as a cause of familial AF. Our findings provide a possible explanation for the variable effectiveness of sodium channel blockers in patients with AF. Carriers of such sodium channel gain-of-function mutations may benefit more from tailored treatments.

Graphical abstract

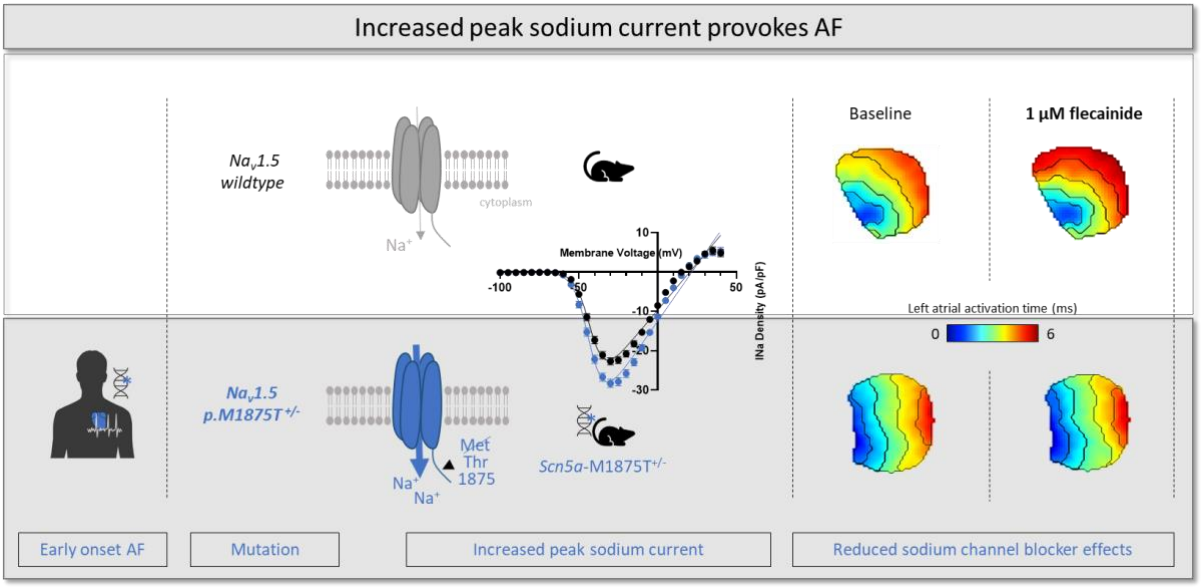

2 Introduction

Atrial fibrillation (AF), the most common cardiac arrhythmia, is characterised by episodes of irregular and uncoordinated atrial electrical activity. It is associated with ischaemic stroke, cardiovascular death and frequent hospitalisations [1]. A range of different common factors, such as heart failure, diabetes and increased formation of fibrosis, can damage the atria, contributing to AF [2, 3]. These factors interact with a pre-existent, potentially inherited substrate to result in AF. Inherited forms are characterised by early onset of the condition. Pathogenic variants in several genes associated with cardiomyopathies have been identified in familial AF, including variants in sarcomeric and cell-cell contact genes, and others [4-6]. Within the group of ion channel genes, variants leading to dysfunction of the cardiac sodium channel are associated with familial AF [4, 7, 8], both via variants in the genes coding for the channel or through upstream mechanisms altering the expression of sodium channel genes [9, 10].

The cardiac voltage-gated sodium channel ($Na_v1.5$) facilitates movement of sodium (Na^+) ions across the cardiomyocyte membrane and hence elicits the cardiac Na^+ current (I_{Na}). I_{Na} is vital for electrical excitation preceding mechanical contraction of the myocardium, as transient influx of Na^+ triggers the fast upstroke phase of the cardiac action potential and thus depolarisation of the cardiomyocyte membrane. The $Na_v1.5$ channel is composed of both α- and ß- subunits. The pore-forming α-subunit is encoded by the *SCN5A* gene. Variants in *SCN5A* have been linked to cardiac conditions, including AF [11-13], Brugada syndrome [14], conduction disease [15-17] and dilated cardiomyopathy [18, 19]. *SCN5A* genetic variants reported [20] show various underlying mechanisms mainly linked to channel dysfunction, defective channel trafficking or protein complex formation [17, 21, 22].

A missense *SCN5A* point mutation, Met1875Thr (M1875T), located in the C-terminus of the channel protein, was linked to autosomal dominant familial AF that spanned three generations of a family [23]. Atrial ectopy was evident in mutation carriers in adolescence, and persistent AF occurred as early as 27 years of age. Analyses in the human cell line HEK293 heterologous expression system [23] suggested an enhanced function of the mutated $Na_v1.5$ channel.

To investigate the impact of the M1875T mutation in a more physiological setting, we generated and characterised a novel knock-in murine model (*Scn5a*-M1875T$^{+/-}$). Mice that were heterozygous for the M1875T mutation were viable and studied herein. We investigated these mice from the whole organ *in vivo* to the level of the single cell *ex vivo*.

3 Methods

3.1 Generation and sequencing of the *Scn5a*-M1875T murine model

Mice heterozygous for the knock-in mutation M1875T in the *Scn5a* gene (*Scn5a*-M1875T$^{+/-}$) were generated by T-C point-mutating exon 28 of the cardiac sodium channel *SCN5A* gene using pSCN5a_targ3 targeting vector and CRISPR/Cas9 system in murine embryonic stem (ES) cells (Figure 1a). Mutation-harboring ES cells were characterised using Southern blot analysis and sequenced in order to exclude genomic rearrangements (Figure 1b) [24, 25], and injected into B6D2F1 mouse blastocysts. Sequencing analysis of the mutation-containing region using DNA from adult wildtype (WT) and heterozygous *Scn5a*-M1875T$^{+/-}$ mice on C57Bl/6J x 129sv hybrid genetic background are shown in Figure 1c. Detailed steps of the generation are further explained in the supplement.

Methionine at position 1875 of the human $Na_v1.5$ protein sequence corresponds to position 1877 of the murine sequence. The latter is therefore point-mutated in this model. However, to underpin the bedside-to-bench nature of this investigation, we use the human annotation and refer to it as "Scn5a-M187**5**T" throughout this manuscript.

Mice were bred on an FVB or 129/sv genetic background and housed in individually ventilated cages with sex-matched littermates (2-5 mice/cage), under standard conditions: 12 hours light/dark circle, 22°C and 55% humidity. Food and water were available *ad libitum*. The health status of mice used in the study was monitored daily and prior to experiments.

Functional experiments were conducted on hearts of male and female young adult mice (8-20 weeks), heterozygous for the knock-in mutation M1875T in the *Scn5a* gene *(Scn5a*-M1875T$^{+/-}$) and their WT littermates.

3.2 Study approval

All procedures were performed in compliance with the guidelines from Directive 2010/63/EU of the European Parliament on the protection of animals used for scientific purposes and conducted in

accordance with rules and regulations for experiments with animals and approved by the UK Home Office (PPL number 30/2967) and by the institutional review board of University of Birmingham.

3.3 Murine ECG recordings *in vivo*

Non-invasive electrocardiograms (ECG) were recorded in conscious young adult mice (8-19 weeks) using a tunnel system for gentle restraint (ecgTunnel, EMKA Technologies, Paris, France) [26]. ECG recordings were analysed using ECGauto software (EMKA Technologies, Paris, France). ECGs were also recorded in sedated mice during echocardiography as below.

3.4 Murine echocardiography *in vivo*

Echocardiography was performed in sedated mice (2% isoflurane, supplemented with 100% O_2) using Vevo® 2100 system (VisualSonics, Amsterdam, Netherlands) as reported previously [27]. Heart rate was maintained at 450 ± 70 bpm. Left atria (LA) were visualised in the parasternal long axis view in the plane of the aortic root. LA area and diameter were measured during pre-atrial contraction, using the P-wave of the limb ECG trace as a guide. Left ventricular parameters were also measured in the parasternal long axis view.

3.5 Left atrial murine cardiomyocyte isolation

Murine hearts were excised under deep terminal anaesthesia (4% isoflurane inhalation in O_2, 1.5 L/min) and perfused at 4 mL.min^{-1} at 37°C on a vertical Langendorff apparatus with the following solutions, equilibrated with 100% O_2: (i) HEPES-buffered, Ca^{2+}-free, modified Tyrode's solution containing in mM: NaCl 145, KCl 5.4, $MgSO_4$ 0.83, Na_2HPO_4 0.33, HEPES 5, and glucose 11 (pH 7.4, NaOH) x 5 min; (ii) Tyrode's enzyme solution containing 640 µg/mL collagenase type II, 600 µg/ml collagenase type IV and 50 µg/ml protease (Worthington, Lakewood, NJ), 20 mM taurine and 3 µM $CaCl_2$ × 8-12 min. The heart was removed from the Langendorff setup and perfused with 5 mL of modified Kraft-Bruhe (KB) solution containing in mM: DL-potassium aspartate 10, L-potassium

glutamate 100, KCl 25, KH_2PO_4 10, $MgSO_4$ 2, taurine 20, creatine 5, EGTA 0.5, HEPES 5, 0.1% BSA, and glucose 20 (pH 7.2, KOH).

The LA was dissected free and cardiomyocytes were dissociated gently with fire-polished glass pipettes (2 to 1 mm diameter in sequence). Cells were re-suspended in 2 mL KB buffer and Ca^{2+} was gradually reintroduced to the cell suspension incrementally over a period of 2 hours to reach a final concentration of 1 mM. All experiments were performed within 8 hours of isolation.

3.6 Whole-cell patch clamp electrophysiology of isolated left atrial cardiomyocytes

Dissociated murine LA cardiomyocytes were plated on, and allowed to adhere to, laminin-coated coverslips (10 mm diameter) for at least 20 minutes. Coverslips were transferred to a recording chamber and were continually superfused at 3 $mL.min^{-1}$, with a low Na^+ external solution containing in mM; NaCl 10, KCl 4.5, $C_5H_{14}ClNO$ 130, $CaCl_2$ 1, $MgCl_2$ 1.2, HEPES 10 and glucose 10 (pH 7.4 with CsOH). To block L-type Ca^{2+} currents, 2 mM $NiCl_2$ was added to the superfusate. Experiments were performed at 22 ± 0.5°C. Whole-cell patch clamp recordings were obtained in voltage-clamp mode using borosilicate glass pipettes (tip resistances 1.5-3 MΩ) [28].

For Na^+ current recordings, the pipette solution contained in mM: CsCl 115, NaCl 5, EGTA 10, HEPES 10, MgATP 5, TEACl 20 and $MgCl_2$ 0.5 (pH 7.2, KOH). Voltage-dependent Na^+ currents were evoked by 5 mV step depolarisations (100 ms) from a holding potential of -100 mV to test potentials ranging from -95 mV to +40 mV. To investigate $Na_v1.5$ voltage-dependent inactivation kinetics, cells were subject to 500 ms pre-pulses ranging from -120 mV to -40 mV, followed by a 100 ms step to -30 mV. For $Na_v1.5$ time-dependent recovery kinetics, a standard two pulse protocol was used (-120 mV to -30 mV, 20 ms), with the time between the two pulses incrementally varying between 5 and 950 ms.

All recordings and analysis protocols were performed using an Axopatch 200B amplifier (Molecular Devices, USA) and digitized at 50 kHz using a CED micro1401 driven by Signal v6 software (Cambridge

Electronic Design, Cambridge, UK). Series resistance was compensated, ranging between 60-100% for all cells. Experiments were terminated if series resistance abruptly changed or was above 10 MΩ.

3.7 Left atrial murine microelectrode recordings

As previously described [28-30], following isolation the LA was immediately transferred into a dissecting chamber and continuously superfused at 10 mL.min^{-1} with a bicarbonate buffered Krebs-Henseleit (KH) solution containing in mM: NaCl 118; $NaHCO_3$ 24.88; KH_2PO_4 1.18; Glucose 11; $MgSO_4$ 0.83; $CaCl_2$ 1.8; KCl 3.52, equilibrated with 95% O_2/5% CO_2, 36-37°C, pH 7.4. Micro-dissection and pinning out of the LA was performed using a dissection microscope (Stemi SV 11, Zeiss, Germany). The LA was paced at 1–10 Hz via bipolar platinum electrodes. Action potentials (APs) were recorded from freely contracting LA using custom made glass floating microelectrodes containing 3 M KCl, (resistance 15-30 MΩ). Voltage signals were amplified and digitised at 20 kHz and were unfiltered (Axoclamp 2B; Molecular Devices, California, USA; Spike2 software Cambridge Electronic Design, Cambridge, UK). Measured parameters included the resting membrane potential (RMP), action potential amplitude (APA), peak depolarisation rate (dV/dt) and action potential duration (APD) at 30-90% repolarisation. APs were only analysed following sufficient rate adaptation achieved after at least 50 stimulated APs at each frequency.

3.8 Optical mapping of murine left atria

Optical mapping of the LA was conducted as previously described [31, 32]. Isolated whole hearts were loaded on to a vertical Langendorff apparatus and perfused with a standard KH solution. Hearts were perfused at 4 mL.min^{-1} (equilibrated with 95%O_2/5%CO_2 and heated to 36-37°C, pH 7.4). Hearts were loaded with 25 µL of voltage sensitive dye Di-4-ANEPPS at a concentration of 5 mg/mL, diluted in 1 mL of KH solution and delivered via bolus port injection over 3-5 minutes. The LA was then isolated and pinned in a superfusion chamber containing 37°C KH solution for transfer to the optical mapping setup, anterior surface facing up.

In the optical mapping system, atria were superfused with KH solution (95%O_2/5%CO_2, 36-37°C) containing contraction uncoupler Blebbistatin (35 µM). For imaging, atria were illuminated by two dual LEDs at 530 nm. A 630 nm long-pass filter was used to sperate emitted fluorescence, imaged using an ORCA flash 4.0 CMOS camera (Hamamatsu, Japan). Images were acquired at a framerate 0.987 kHz and pixel size of 71 µm/pixel^2. Atria were paced using bipolar platinum electrodes delivering 2 ms pulses at twice diastolic threshold (minimum voltage required to elicit APs).

One-minute baseline recording was taken following a 10 minutes equilibration period to ensure contraction uncoupling and temperature re-stabilisation. During imaging, atria were initially paced at 330 ms pacing cycle length (PCL). A 'ramp' pacing protocol was then initiated, in which the atria were paced at 120 ms PCL for 100 stimuli and then PCL was reduced from 120 ms to 80 ms in 10 ms intervals every 20 stimuli. After taking baseline recordings, LED illumination was switched off and the superfusion solution replaced with an identical solution containing flecainide at a concentration of 1 µM and then 5 µM (or control solution without flecainide for time control experiments). Subsequent recordings were then made as described above after 20 minutes superfusion with 1 µM flecainide solution, and then further 15 minutes with 5 µM flecainide solution. Atria were paced at 330 ms PCL continuously in dark conditions between recordings.

From these recordings, APD and conduction velocity (CV) were mapped across the LA using ElectroMap software [32]. Atria were removed from analysis at a given PCL if loss of 1:1 capture ratio with pacing stimuli (i.e. missed beats) was observed.

3.9 Statistics

For all murine experiments presented herein, experimenters were blinded to the genotype of the littermate pairs during data collection and analysis. Student t-tests were used for singular comparisons for normally distributed data. A hierarchical nested t-test (Figure 2) and Mann-Whitney test (Supplementary Table 3) were used where appropriate. Multiple comparisons were made using 2-way ANOVA with Bonferroni's post-hoc tests. For current-voltage graphs (Figure 2b), a Boltzmann curve

was fit to the data. All graphical representations display individual measurements. Means are quoted and shown in Figures ± SEM. Level of statistical significance is shown in Figures as follows: *p<0.05; **p<0.01; ***p<0.001; ****p<0.0001. Statistics and Figures were created using Prism 8 (GraphPad Software, San Diego, California).

4 Results

4.1 Viable heterozygous *Scn5a*-M1875T$^{+/-}$ mice show normal cardiac size and basic function

The point mutation previously identified in patients with early familial AF was successfully introduced to exon 28 of the mouse *Scn5a* gene via homologous recombination of a targeting vector. The vector contained the T-C point mutation (CRISPR/cas9-mediated) resulting in methionine-threonine exchange in the $Na_v1.5$ protein (Figure 1). Offspring from both WT x heterozygote (=*Scn5a*-M1875T$^{+/-}$) and heterozygote x heterozygote pairings were viable. No homozygous *Scn5a*-M1875T$^{-/-}$ offspring was born (Supplementary Figure 1b), suggesting embryonic lethality, as previously reported for other *Scn5a* mutations [33, 34]. Accordingly, the ratio of WT and heterozygous animals shifted from 1:2 (expected) to approximately 1:3 when heterozygous animals were crossed (Supplementary Figure 1b). The ratio of male:female sex in offspring approximated 1:1 as expected (Supplementary Figure 1c).

Age-matched young adult WT and *Scn5a*-M1875T$^{+/-}$ mice displayed similar heart rate, PR-, QRS- and QT- interval regardless of genotype in electrocardiograms recorded awake (Supplementary Table 1) and during sedation (Supplementary Table 2). Echocardiography and histological examination excluded overt differences in atrial or ventricular structure (Supplementary Table 3, Supplementary Figure 2a). Accordingly, pro atrial natriuretic peptide (proANP) was detected in right atria as expected but was not elevated in ventricles (Supplementary Figure 2b).

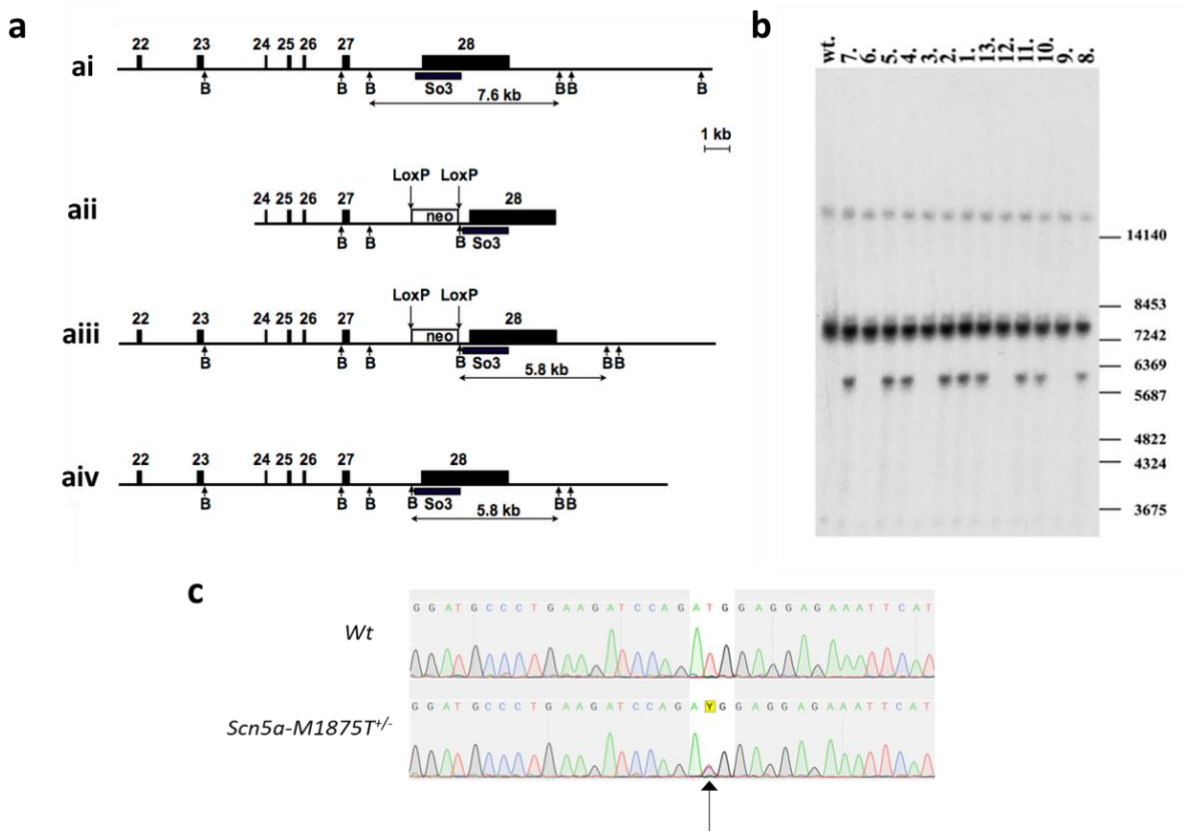

Figure 1 Targeting of exon 28 of the mouse *Scn5a* gene in order to introduce the M1875T coding mutation, and sequencing confirmation of its presence

a) The intronic and intergenic regions are shown as lines, exons are shown as filled boxes. The empty box corresponds to the neomycin resistance cassette (neo) flanked by the LoxP sites (vertical arrows). Exon numeration is shown above. The arrows below are corresponding to BamHI restriction endonuclease sites (B). The black box corresponds to Southern probe sequences (So3). The expected sizes of restriction DNA fragments are indicated below in kb. **ai)** Wildtype (WT) locus. **aii)** Targeted vector structure (without negative selection marker and plasmid backbone). **aiii)** Genomic locus after the homologous recombination. The neomycin cassette is present in intron 27 and flanked by two LoxP sites. **aiv)** Genomic locus after the CRE-mediated neo cassette deletion. **b)** Southern blot analysis of DNA isolated from mouse tail biopsy of the F1 offspring (1-13) and hybridized with the So3 probe. With help of the BamHI enzymatic digestion, we detect the WT allele 7.6 kb and targeted allele 5.8 kb. DNA samples 1, 2, 4, 5, 7, 8, 10, 11, and 13 contain correctly targeted *Scn5a* gene (Scn5a-M1875T$^{+/-}$). Positions of the size marker (in bp) are shown on the right. The WT control animal is labeled "wt.". **c)** Sequencing analysis of the *Scn5a* gene region containing the mutation site in back-crossed adult mice (on pure genetic background). The T-C mutation on one allele causing the methionine-threonine exchange at position 1875 (1877) is indicated by an arrow.

4.2 Atrial *Scn5a*-M1875T$^{+/-}$ cardiomyocytes have an augmented peak sodium current density

To determine the impact of the M1875T point mutation on peak I_{Na} amplitude and $Na_v1.5$ channel gating properties, left atrial cardiomyocytes from WT and *Scn5a*-M1875T$^{+/-}$ mice (8-13 weeks) were isolated and whole-cell patch clamp recordings were performed.

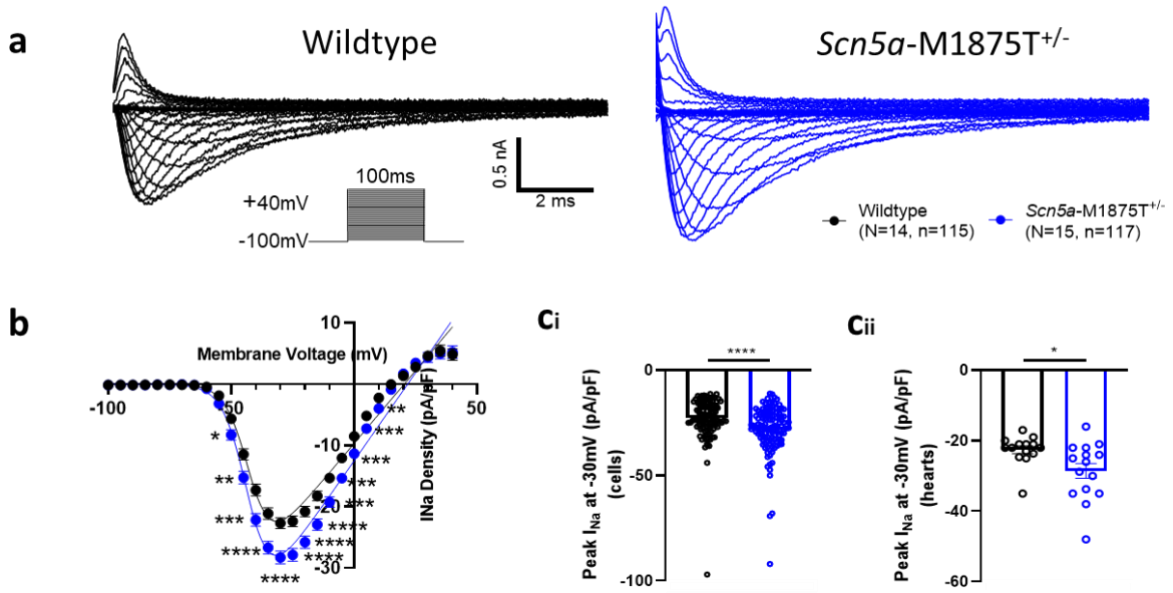

Figure 2 Isolated left atrial cardiomyocytes with the *Scn5a*-M1875T$^{+/-}$ mutation have a larger sodium current than wildtypes when measured with whole-cell patch clamp electrophysiology
a) Representative sodium current (I_{Na}) traces from whole-cell voltage clamp recording of isolated left atrial (LA) cardiomyocytes from wildtype (WT) (black) and *Scn5a*-M1875T$^{+/-}$ (blue) mice. **b)** Normalised grouped data revealed that the *Scn5a*-M1875T$^{+/-}$ mutation increases peak I_{Na} in LA cardiomyocytes over test potentials ranging from –100 to +40 mV. **c)** At the peak I_{Na} test potential of -30 mV, *Scn5a*-M1875T$^{+/-}$ cardiomyocytes had a significantly larger I_{Na} than WTs, both when comparing individual cells (n=115 WT, n=117 *Scn5a*-M1875T$^{+/-}$) **(ci)** and animals (N=14 WT, N=15 *Scn5a*-M1875T$^{+/-}$) **(cii)**.

The M1875T variant increased I_{Na} over test potentials ranging from –100 to +40 mV (Figure 2a and b). At a peak test potential of -30 mV, mean left atrial cardiomyocyte I_{Na} density was higher in *Scn5a*-M1875T$^{+/-}$ (-28.3 ± 1.1 pA/pF, n=117 cells) than in WT littermates (-22.7 ± 0.9 pA/pF, n=115 cells, p<0.0001, Figure 2ci). The elevation in I_{Na} was also apparent when recordings were grouped by animal (*Scn5a*-M1875T$^{+/-}$ -27.7 ± 2.1 pA/pF, N=15 vs WT -22.3 ± 1.2 pA/pF, N=14, p=0.039, Figure 2cii) and after applying hierarchical analysis (*Scn5a*-M1875T$^{+/-}$ -28.3 ± 1.1 pA/pF, n=117 cells, N=15 mice vs WT -22.7 ± 0.9 pA/pF, n=115 cells, N=14 mice, p=0.016).

Capacitance measurements were not different between genotypes, indicative of similar cell size (Supplementary Figure 3a).

Whole-cell I_{Na} voltage-dependent inactivation and time-dependent recovery kinetics were not altered in *Scn5a*-M1875T$^{+/-}$ cardiomyocytes compared to WT (Supplementary Figure 3b and c). $Na_v1.5$

expression in hearts of *Scn5a*-M1875T$^{+/-}$ mice at mRNA and the protein level revealed no difference at either the whole cell or isolated membrane fraction level (Supplementary Figure 4).

4.3 Intact *Scn5a*-M1875T$^{+/-}$ left atria have a larger action potential amplitude and faster peak upstroke velocity

To further characterise the impact of the M1875T variant on cardiac electrophysiology, action potentials (APs) were measured in whole left atrial tissue isolated from WT and *Scn5a*-M1875T$^{+/-}$ mice (9-13 weeks) using sharp microelectrodes. Representative AP traces are shown in Figure 3 during stimulation at 100 ms (Figure 3c) and 1000 ms pacing cycle length (PCL) (Figure 3f).

Action potential amplitude was significantly larger in *Scn5a*-M1875T$^{+/-}$ murine left atria at all PCLs tested and this effect was more pronounced at shorter cycle lengths (N=8, n=24-25, Figure 3a). The variant resulted in a faster peak upstroke velocity (dV/dt), especially at the shorter cycle lengths (100 ms PCL: WT 128.0 ± 3.3, n=24; *Scn5a*-M1875T$^{+/-}$ 142.8 ± 4.0 mV/ms, n=25, p=0.0282, Figure 3b).

The resting membrane potential [35] was not different between genotypes (100 ms PCL: WT -72.4 ± 0.6; *Scn5a*-M1875T$^{+/-}$ -73.1 ± 0.6 mV). Atrial activation times were also similar (100 ms PCL: WT 4.9 ± 0.2; *Scn5a*-M1875T+/- 4.9 ± 0.2 ms) (Supplementary Table 4). Only at the long PCL of 1000 ms, the AP duration (APD) at 50 and 90% repolarisation was shorter in *Scn5a*-M1875T$^{+/-}$ left atria than in WT (Figure 3d and e), while the APD at 30 and 70% repolarisation was not significantly different (Supplementary Table 4). Similarly, optical mapping data showed no APD differences at PCLs tested.

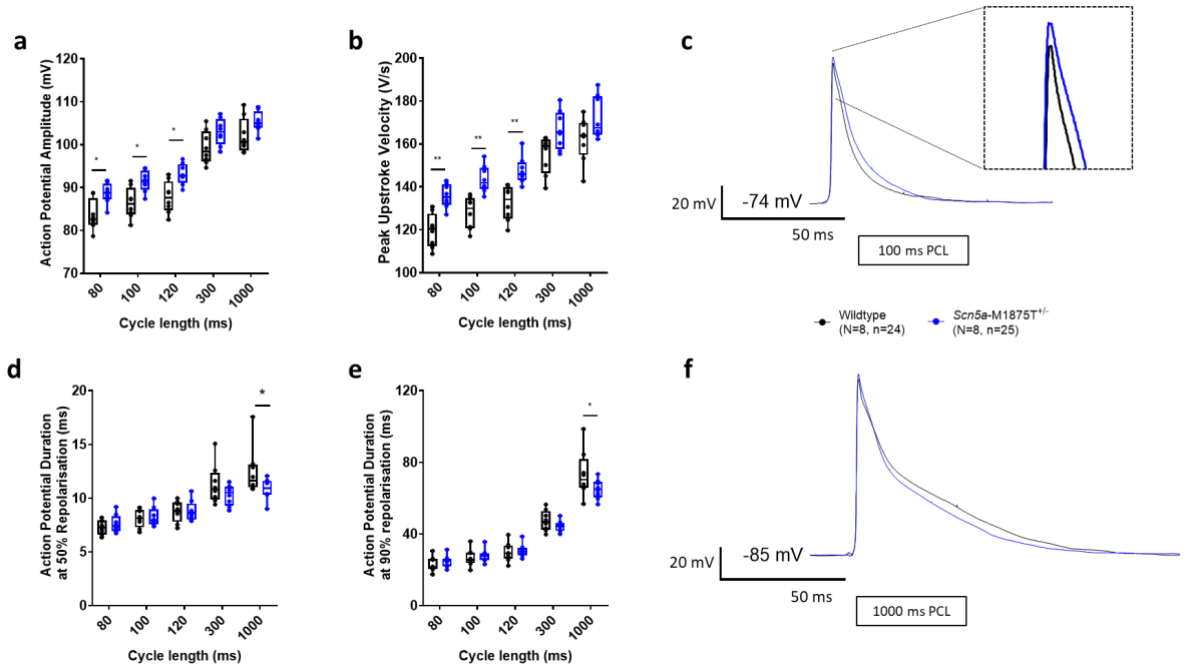

Figure 3 Left atria with the *Scn5a*-M1875T$^{+/-}$ mutation have a larger action potential amplitude and a faster peak upstroke velocity when measured with the sharp microelectrode technique
a) *Scn5a*-M1875T$^{+/-}$ left atria (LA) had a significantly larger action potential (AP) amplitude at shorter pacing cycle lengths (PCLs) of 80-120 ms ($p<0.05$) and **b)** a significantly faster peak upstroke velocity (dV/dt). **d-f)** When paced at 1000 ms PCL, *Scn5a*-M1875T$^{+/-}$ LA had a significantly shorter AP duration (APD) when measured at 50% (APD50) **(d)** and 90% (APD90) **(e)** repolarisation. *$p<0.05$, **$p<0.01$, wildtype (WT) vs *Scn5a*-M1875T$^{+/-}$, N=8 per group, n=24 WT, n=25 *Scn5a*-M1875T$^{+/-}$; ANOVA statistics. Also shown are representative AP traces from wildtype (black) and *Scn5a*-M1875T$^{+/-}$ (blue) LA when stimulated at 100 ms **(c)** and 1000 ms PCL **(f)**.

4.4 Flecainide-induced atrial conduction slowing and post-repolarisation refractoriness is less pronounced in *Scn5a*-M1875T$^{+/-}$ left atria

Optical mapping of WT and *Scn5a*-M1875T$^{+/-}$ whole left atrial tissue was performed to test effects of the heterozygous *Scn5a*-M1875T mutation on atrial conduction.

Left atria were superfused with the open channel sodium channel blocker flecainide (1 µM, clinically used concentration) to determine the response of *Scn5a*-M1875T$^{+/-}$ and WT left atria. While conduction velocity was unchanged at baseline, flecainide slowed conduction less in *Scn5a*-M1875T$^{+/-}$

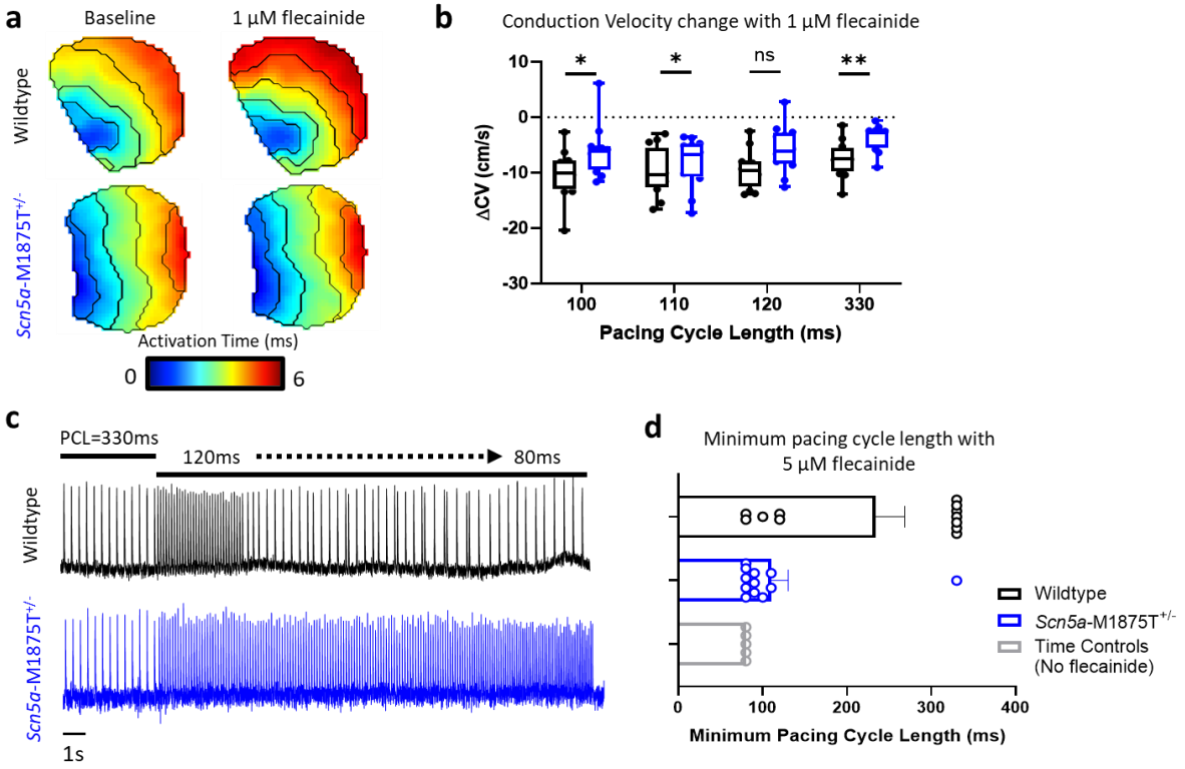

Figure 4 Left atria with the *Scn5a*-M1875T$^{+/-}$ mutation have a reduced response to the anti-arrhythmic agent flecainide in optical mapping

a) Example left atrial (LA) activation maps from wildtype (WT, top panels) and *Scn5a*-M1875T$^{+/-}$ (bottom panels) mice. Left panels show activation maps at baseline, right panels show activation of the same atria following exposure to 1 µM flecainide for 20 minutes. **b)** Grouped data showing change in conduction velocity (ΔCV) following exposure to 1 µM flecainide in WT (black) and *Scn5a*-M1875T$^{+/-}$ (blue) LA for 20 mins. **c)** Example traces of optical action potentials (APs) recorded following further treatment of WT (top, black) and *Scn5a*-M1875T$^{+/-}$ (bottom, blue) LA with 5 µM flecainide for 15 mins. **d)** Grouped data showing minimum pacing cycle length (PCL) at which 1:1 stimulus capture was maintained in WT (black) and *Scn5a*-M1875T$^{+/-}$ (blue) LA following exposure to 5 µM flecainide. Time control data (grey) shows minimum PCL at which 1:1 stimulus capture was maintained in atria that were not exposed to flecainide but had been under experiment conditions for the same time period (35 mins from baseline recording). N=12 per group at 330 ms-100 ms PCL. Atria were excluded from further analysis at shorter PCLs if 1:1 capture was lost, only data in steady state was used. N=5 for time control experiments. *p<0.05, **p<0.01, WT vs *Scn5a*-M1875T$^{+/-}$; ANOVA statistics.

left atria (conduction velocity difference at 100 ms PCL -6 ± 1 cm/s, n=12, p=0.0357) than in WTs (conduction velocity difference at 100 ms PCL -10 ± 1 cm/s, n=12, p=0.0357, Figure 4a and b). We also investigated flecainide-induced changes in left atrial refractoriness as it is known that flecainide induces post-repolarisation refractoriness using rapid atrial pacing. Representative optical AP recordings show 1:1 capture in the *Scn5a*-M1875T$^{+/-}$ left atria with flecainide, while several stimuli in the WT left atria did not elicit APs (Figure 4c). All time-controlled left atria (no flecainide, same

247 experimental duration) were successfully paced with 1:1 capture down to 80 ms PCL. Loss of 1:1
248 capture began at longer PCLs in WT (7/12 atria lost 1:1 capture at PCLs ≤ 120 ms) compared to *Scn5a*-
249 M1875T$^{+/-}$ (1/12 atria lost 1:1 capture at PCLs ≤ 120 ms, p=0.0185) left atria. The diastolic pacing
250 threshold remained consistent throughout experiments. Thus, flecainide induced less pronounced
251 post-repolarisation refractoriness in the *Scn5a*-M1875T$^{+/-}$ left atria.

5 Discussion

5.1 Main findings

Our study describes the effects of the familial atrial fibrillation (AF) mutation *Scn5a*-M1875T$^{+/-}$ in a newly generated murine model. Key effects are that the M1875T *Scn5a* mutation leads to an increased action potential upstroke velocity and amplitude and a selective increase in the early cardiac sodium current (I_{Na}) while cardiomyocyte capacitance, and cardiac size and function are preserved. *Scn5a*-M1875T$^{+/-}$ left atria exhibit a dampened effect to the sodium channel blocker flecainide. Our data in this new murine model suggest that a selective increase of I_{Na} can cause familial AF, and that commonly used concentrations of sodium channel blockers may be less effective in familial forms of AF with a selective increase in I_{Na} than in other types.

5.2 Novel gain-of-function properties of M1875T sodium channels in the murine left atrium

Our data confirm a gain-of-function variant, namely an increased early sodium current as evidenced by an augmented action potential amplitude and larger I_{Na} in the *Scn5a*-M1875T$^{+/-}$ variant.

In contrast to findings in HEK293 cells [23], there was no leftward shift of channel activation in murine left atrial cardiomyocytes. Instead, we show a similarly augmented I_{Na} without alterations in channel gating properties. Generation of the murine mutant model allowed us to study mutated sodium channels in cardiac tissue within the presence of the greater protein complex including α- and β-subunits and other membrane proteins, a complete cardiomyocyte contractile apparatus and all other cardiac cell types. In contrast, HEK293 cells would not contract, exclusively contained the mutated version of $Na_v1.5$ in their membranes and are by necessity studied in isolation. Others have reported similar differences between HEK293 and cardiac model systems to the differences reported here [36]. Cardiac sodium channels have been observed to form dimers and structural analysis following the hypothesis of $Na_v1.5$ dimerization via C-terminal interaction reveals that the surface of residue

Met1875 of one $Na_v1.5$ cytosolic C-terminus will interact with Ala1924 of a second $Na_v1.5$ [37]. This prediction highlights the importance of the location site investigated in our model as it could provide a structural basis for altered $Na_v1.5$-$Na_v1.5$ channel interaction further to be investigated.

5.3 Genotype-phenotype relationship of the *Scn5a*-M1875T$^{+/-}$ mutation

Propagation of action potentials (APs) is carefully orchestrated throughout the atria to ensure effective cardiac function. Disturbed, inhomogeneous electrical activation or altered repolarisation can increase the propensity for re-entrant electrical circuits leading to atrial arrhythmias [38, 39]. Defects in conduction velocity, resulting in slow or inhomogeneous conduction, occur due to altered depolarisation and repolarisation kinetics. While structural alterations of the atria, summarised as atrial cardiomyopathy, often contribute to atrial conduction disturbances [40], defects in the cardiac sodium channel can also cause conduction defects leading to AF [17-22].

Unlike other *SCN5A* mutations [17-22], this variant shows a dampened response to flecainide both on conduction and post-repolarisation refractoriness [41]. Flecainide is a clinically used sodium channel blocker that inhibits cardiac I_{Na} via blocking the pores of open $Na_v1.5$ channels [42, 43]. The effects of flecainide were reduced in *Scn5a*-M1875T$^{+/-}$ atria when compared to wildtype. This differential response to flecainide is likely due to the increased early sodium influx through the mutated $Na_v1.5$ channels, enabling preservation of conduction and activation properties in atrial cardiomyocytes when sodium channels are inhibited, leading to an enhanced activation reserve.

Murine models have limitations due to differences between mice and men, but they have been useful in characterising sodium channel mutations [27, 33, 34, 44]. Identified mutation-induced changes at the cellular and organ level in this model appear sufficient to explain AF in the original family.

It is unlikely that the M1875T mutation increases the late sodium current ($I_{Na,l}$), as APs we measured were not prolonged by the mutation, in line with the initial report of the mutation in HEK cells [23]. A lack of AP prolongation clearly differs to findings in the *ΔKPQ-Scn5a* mutant murine model showing a selective increase in $I_{Na,l}$ [27, 28, 33]. The gain-of-function mutation *ΔKPQ-SCN5A* resulted in prolonged atrial and ventricular AP duration, especially at longer pacing cycle lengths. This suggests that the M1875T mutation acts differently to, and is distinct from, *SCN5A* gain-of-function mutations leading to prolonged repolarisation and long QT syndrome, in concordance with the broad spectrum of phenotypic outcomes resulting from mutations in the same ion channel gene [45].

An enhanced sodium influx into cardiomyocytes will alter the sodium-calcium homeostasis [46, 47], modifying intracellular sodium and calcium concentrations and signalling in cardiomyocyte microdomains [48, 49]. This study found normal heart size and cardiomyocyte size. Nonetheless, chronic sodium overload can result in structural changes in the heart with ageing. In the future, the M1875T mouse model may be used to study the long-term effects of a selective increase in the early I_{Na}. Studies in human cardiomyocytes [47] and in atrial engineered heart tissue [50, 51], would be desirable to assess the effect of the M1875T mutation in human models in the future.

Conclusion

The *Scn5a*-M1875T$^{+/-}$ variant causes a selective increase in the early cardiac sodium current, potentially leading to an increased activation reserve, whilst structure and contractile function are preserved. These findings can explain the familial occurrence of atrial ectopy and atrial fibrillation in the absence of reported severe heart disease and provide a novel mechanism by which altered cardiomyocyte sodium currents can predispose to atrial fibrillation. Our data also suggest that the M1875T gain-of-function mutation decreases the effectiveness of sodium channel blockers such as flecainide, which may have implications for patient treatment.

Data availability

The data underlying this article will be shared on reasonable request to the corresponding author. The software code on which part of the conclusions of this paper rely is available at https://github.com/CXO531/ElectroMap (O´Shea C, Yu TY; December 21st 2018; ElectroMap; GitHub).

Funding

This work was partially supported by the Leducq Foundation, British Heart Foundation [FS/12/40/29712; FS/13/43/30324; PG/17/30/32961; PG/20/22/35093; AA/18/2/34218], EU Horizon 2020 CATCH ME (grant agreement number 633196), AFFECT-EU [grant agreement number 847770] and MAESTRIA [grant agreement number 965286], European Union BigData@Heart [grant agreement EU IMI 116074], German Centre for Cardiovascular Research supported by the German Ministry of Education and Research (DZHK), Medical Research Council [MR/V009540/1], and the Wellcome Trust [201543/B/16/Z; 221650/Z/20/Z].

Author Contribution Statement

LF and PK designed the research; BVS generated the mouse model in TRAM upon request by PK and LF;

MO, LCS, CO, SBS, SA, JSR, SNK, AM, DD, LFo, LF and APH conducted experiments, analysed data and performed statistical analysis;

KG, DP, APH, PK, LF supervised experiments and analysis.

MO, LCS, CO, SBS and LF wrote the manuscript together with all co-authors. All co-authors critically reviewed the manuscript.

Acknowledgments

We thank Hartwig Wieboldt, Daniel Stastny, Clara Apicella and Olivia Grech for technical assistance.

Conflict of Interest

The authors have declared no direct conflict of interest in regards to the manuscript.

L.F. has received institutional research grants from governmental and charity funding agencies and several biomedical companies.

P.K. has received research support from several drug and device companies active in atrial fibrillation and has received honoraria from several such companies in the past.

L.F. and P.K. are listed as inventors on two patents held by University of Birmingham (Atrial Fibrillation Therapy WO 015140571, Markers for Atrial Fibrillation WO 2016012783).

References

1. Fabritz L, Crijns H, Guasch E, Goette A, Hausler KG, Kotecha D, Lewalter T, Meyer C, Potpara TS, Rienstra M, Schnabel RB, Willems S, Breithardt G, Camm AJ, Chan A, Chua W, de Melis M, Dimopoulou C, Dobrev D, Easter C, Eckardt L, Haase D, Hatem S, Healey JS, Heijman J, Hohnloser SH, Huebner T, Ilyas BS, Isaacs A, Kutschka I, Leclercq C, Lip GYH, Marinelli EA, Merino JL, Mont L, Nabauer M, Oldgren J, Purerfellner H, Ravens U, Savelieva I, Sinner MF, Sitch A, Smolnik R, Steffel J, Stein K, Stoll M, Svennberg E, Thomas D, Van Gelder IC, Vardar B, Wakili R, Wieloch M, Zeemering S, Ziegler PD, Heidbuchel H, Hindricks G, Schotten U, Kirchhof P. Dynamic risk assessment to improve quality of care in patients with atrial fibrillation: the 7th AFNET/EHRA Consensus Conference. *Europace* 2021;**23**:329-344.
2. Fabritz L, Guasch E, Antoniades C, Bardinet I, Benninger G, Betts TR, Brand E, Breithardt G, Bucklar-Suchankova G, Camm AJ, Cartlidge D, Casadei B, Chua WW, Crijns HJ, Deeks J, Hatem S, Hidden-Lucet F, Kaab S, Maniadakis N, Martin S, Mont L, Reinecke H, Sinner MF, Schotten U, Southwood T, Stoll M, Vardas P, Wakili R, West A, Ziegler A, Kirchhof P. Expert consensus document: Defining the major health modifiers causing atrial fibrillation: a roadmap to underpin personalized prevention and treatment. *Nat Rev Cardiol* 2016;**13**:230-237.
3. Benjamin EJ, Al-Khatib SM, Desvigne-Nickens P, Alonso A, Djousse L, Forman DE, Gillis AM, Hendriks JML, Hills MT, Kirchhof P, Link MS, Marcus GM, Mehra R, Murray KT, Parkash R, Pina IL, Redline S, Rienstra M, Sanders P, Somers VK, Van Wagoner DR, Wang PJ, Cooper LS, Go AS. Research Priorities in the Secondary Prevention of Atrial Fibrillation: A National Heart, Lung, and Blood Institute Virtual Workshop Report. *J Am Heart Assoc* 2021:e021566.
4. Chalazan B, Mol D, Darbar FA, Ornelas-Loredo A, Al-Azzam B, Chen Y, Tofovic D, Sridhar A, Alzahrani Z, Ellinor P, Darbar D. Association of Rare Genetic Variants and Early-Onset Atrial Fibrillation in Ethnic Minority Individuals. *JAMA Cardiol* 2021.
5. Gudbjartsson DF, Holm H, Sulem P, Masson G, Oddsson A, Magnusson OT, Saemundsdottir J, Helgadottir HT, Helgason H, Johannsdottir H, Gretarsdottir S, Gudjonsson SA, Njolstad I, Lochen ML, Baum L, Ma RC, Sigfusson G, Kong A, Thorgeirsson G, Sverrisson JT, Thorsteinsdottir U, Stefansson K, Arnar DO. A frameshift deletion in the sarcomere gene MYL4 causes early-onset familial atrial fibrillation. *Eur Heart J* 2017;**38**:27-34.
6. Hodgson-Zingman DM, Karst ML, Zingman LV, Heublein DM, Darbar D, Herron KJ, Ballew JD, de Andrade M, Burnett JC, Jr., Olson TM. Atrial natriuretic peptide frameshift mutation in familial atrial fibrillation. *N Engl J Med* 2008;**359**:158-165.
7. Ellinor PT, Nam EG, Shea MA, Milan DJ, Ruskin JN, MacRae CA. Cardiac sodium channel mutation in atrial fibrillation. *Heart Rhythm* 2008;**5**:99-105.
8. Johnson JN, Tester DJ, Perry J, Salisbury BA, Reed CR, Ackerman MJ. Prevalence of early-onset atrial fibrillation in congenital long QT syndrome. *Heart Rhythm* 2008;**5**:704-709.
9. Rivaud MR, Delmar M, Remme CA. Heritable arrhythmia syndromes associated with abnormal cardiac sodium channel function: ionic and non-ionic mechanisms. *Cardiovasc Res* 2020;**116**:1557-1570.

10. van Ouwerkerk AF, Bosada FM, Liu J, Zhang J, van Duijvenboden K, Chaffin M, Tucker NR, Pijnappels D, Ellinor PT, Barnett P, de Vries AAF, Christoffels VM. Identification of Functional Variant Enhancers Associated With Atrial Fibrillation. *Circ Res* 2020;**127**:229-243.
11. Chen LY, Ballew JD, Herron KJ, Rodeheffer RJ, Olson TM. A common polymorphism in SCN5A is associated with lone atrial fibrillation. *Clin Pharmacol Ther* 2007;**81**:35-41.
12. Benito B, Brugada R, Perich RM, Lizotte E, Cinca J, Mont L, Berruezo A, Tolosana JM, Freixa X, Brugada P, Brugada J. A mutation in the sodium channel is responsible for the association of long QT syndrome and familial atrial fibrillation. *Heart Rhythm* 2008;**5**:1434-1440.
13. Darbar D, Kannankeril PJ, Donahue BS, Kucera G, Stubblefield T, Haines JL, George AL, Jr., Roden DM. Cardiac sodium channel (SCN5A) variants associated with atrial fibrillation. *Circulation* 2008;**117**:1927-1935.
14. Alings M, Wilde A. "Brugada" syndrome: clinical data and suggested pathophysiological mechanism. *Circulation* 1999;**99**:666-673.
15. Schott J-J, Alshinawi C, Kyndt F, Probst V, Hoorntje TM, Hulsbeek M, Wilde AAM, Escande D, Mannens MMAM, Le Marec H. Cardiac conduction defects associate with mutations in SCN5A. *Nat Genet* 1999;**23**:20-21.
16. Tan HL, Bink-Boelkens MT, Bezzina CR, Viswanathan PC, Beaufort-Krol GC, van Tintelen PJ, van den Berg MP, Wilde AA, Balser JR. A sodium-channel mutation causes isolated cardiac conduction disease. *Nature* 2001;**409**:1043-1047.
17. Zumhagen S, Veldkamp MW, Stallmeyer B, Baartscheer A, Eckardt L, Paul M, Remme CA, Bhuiyan ZA, Bezzina CR, Schulze-Bahr E. A heterozygous deletion mutation in the cardiac sodium channel gene SCN5A with loss- and gain-of-function characteristics manifests as isolated conduction disease, without signs of Brugada or long QT syndrome. *PLoS One* 2013;**8**:e67963.
18. Hesse M, Kondo CS, Clark RB, Su L, Allen FL, Geary-Joo CT, Kunnathu S, Severson DL, Nygren A, Giles WR, Cross JC. Dilated cardiomyopathy is associated with reduced expression of the cardiac sodium channel Scn5a. *Cardiovasc Res* 2007;**75**:498-509.
19. Remme CA, Bezzina CR. Sodium channel (dys)function and cardiac arrhythmias. *Cardiovasc Ther* 2010;**28**:287-294.
20. Wang T, Wehrens XH. Enhanced impact of SCN5A mutation associated with long QT syndrome in fetal splice isoform. *Heart Rhythm* 2012;**9**:598-599.
21. Rivolta I, Abriel H, Tateyama M, Liu H, Memmi M, Vardas P, Napolitano C, Priori SG, Kass RS. Inherited Brugada and long QT-3 syndrome mutations of a single residue of the cardiac sodium channel confer distinct channel and clinical phenotypes. *J Biol Chem* 2001;**276**:30623-30630.
22. Clerx M, Heijman J, Collins P, Volders PGA. Predicting changes to INa from missense mutations in human SCN5A. *Sci Rep* 2018;**8**:12797.
23. Makiyama T, Akao M, Shizuta S, Doi T, Nishiyama K, Oka Y, Ohno S, Nishio Y, Tsuji K, Itoh H, Kimura T, Kita T, Horie M. A novel SCN5A gain-of-function mutation M1875T associated with familial atrial fibrillation. *J Am Coll Cardiol* 2008;**52**:1326-1334.
24. Skryabin BV, Kummerfeld DM, Gubar L, Seeger B, Kaiser H, Stegemann A, Roth J, Meuth SG, Pavenstädt H, Sherwood J, Pap T, Wedlich-Söldner R, Sunderkötter C, Schwartz YB, Brosius J, Rozhdestvensky TS. Pervasive head-to-tail insertions of DNA templates mask desired CRISPR-Cas9-mediated genome editing events. *Sci Adv* 2020;**6**:eaax2941.

25. Smirnov A, Fishman V, Yunusova A, Korablev A, Serova I, Skryabin BV, Rozhdestvensky TS, Battulin N. DNA barcoding reveals that injected transgenes are predominantly processed by homologous recombination in mouse zygote. *Nucleic Acids Res* 2020;**48**:719-735.
26. Silbernagel N, Walecki M, Schafer MK, Kessler M, Zobeiri M, Rinne S, Kiper AK, Komadowski MA, Vowinkel KS, Wemhoner K, Fortmuller L, Schewe M, Dolga AM, Scekic-Zahirovic J, Matschke LA, Culmsee C, Baukrowitz T, Monassier L, Ullrich ND, Dupuis L, Just S, Budde T, Fabritz L, Decher N. The VAMP-associated protein VAPB is required for cardiac and neuronal pacemaker channel function. *FASEB J* 2018;**32**:6159-6173.
27. Blana A, Kaese S, Fortmüller L, Laakmann S, Damke D, van Bragt K, Eckstein J, Piccini I, Kirchhefer U, Nattel S, Breithardt G, Carmeliet P, Carmeliet E, Schotten U, Verheule S, Kirchhof P, Fabritz L. Knock-in gain-of-function sodium channel mutation prolongs atrial action potentials and alters atrial vulnerability. *Heart Rhythm* 2010;**7**:1862-1869.
28. Lemoine MD, Duverger JE, Naud P, Chartier D, Qi XY, Comtois P, Fabritz L, Kirchhof P, Nattel S. Arrhythmogenic left atrial cellular electrophysiology in a murine genetic long QT syndrome model. *Cardiovascular research* 2011;**92**:67-74.
29. Holmes AP, Yu TY, Tull S, Syeda F, Kuhlmann SM, O'Brien SM, Patel P, Brain KL, Pavlovic D, Brown NA, Fabritz L, Kirchhof P. A Regional Reduction in Ito and IKACh in the Murine Posterior Left Atrial Myocardium Is Associated with Action Potential Prolongation and Increased Ectopic Activity. *PLoS One* 2016;**11**:e0154077.
30. Syeda F, Holmes AP, Yu TY, Tull S, Kuhlmann SM, Pavlovic D, Betney D, Riley G, Kucera JP, Jousset F, de Groot JR, Rohr S, Brown NA, Fabritz L, Kirchhof P. PITX2 Modulates Atrial Membrane Potential and the Antiarrhythmic Effects of Sodium-Channel Blockers. *J Am Coll Cardiol* 2016;**68**:1881-1894.
31. Yu TY, Syeda F, Holmes AP, Osborne B, Dehghani H, Brain KL, Kirchhof P, Fabritz L. An automated system using spatial oversampling for optical mapping in murine atria. Development and validation with monophasic and transmembrane action potentials. *Prog Biophys Mol Biol* 2014;**115**:340-348.
32. O'Shea C, Holmes AP, Yu TY, Winter J, Wells SP, Correia J, Boukens BJ, De Groot JR, Chu GS, Li X, Ng GA, Kirchhof P, Fabritz L, Rajpoot K, Pavlovic D. ElectroMap: High-throughput open-source software for analysis and mapping of cardiac electrophysiology. *Sci Rep* 2019;**9**:1389.
33. Nuyens D, Stengl M, Dugarmaa S, Rossenbacker T, Compernolle V, Rudy Y, Smits JF, Flameng W, Clancy CE, Moons L, Vos MA, Dewerchin M, Benndorf K, Collen D, Carmeliet E, Carmeliet P. Abrupt rate accelerations or premature beats cause life-threatening arrhythmias in mice with long-QT3 syndrome. *Nat Med* 2001;**7**:1021-1027.
34. Remme CA, Verkerk AO, Nuyens D, van Ginneken AC, van Brunschot S, Belterman CN, Wilders R, van Roon MA, Tan HL, Wilde AA, Carmeliet P, de Bakker JM, Veldkamp MW, Bezzina CR. Overlap syndrome of cardiac sodium channel disease in mice carrying the equivalent mutation of human SCN5A-1795insD. *Circulation* 2006;**114**:2584-2594.
35. Holmes AP, Saxena P, Kabir SN, O'Shea C, Kuhlmann SM, Gupta S, Fobian D, Apicella C, O'Reilly M, Syeda F, Reyat JS, Smith GL, Workman AJ, Pavlovic D, Fabritz L, Kirchhof P. Atrial resting membrane potential confers sodium current sensitivity to propafenone, flecainide, and dronedarone. *Heart Rhythm* 2021.

36. Casini S, Albesa M, Wang Z, Portero V, Ross-Kaschitza D, Rougier JS, Marchal GA, Chung WK, Bezzina CR, Abriel H, Remme CA. Functional Consequences of the SCN5A-p.Y1977N Mutation within the PY Ubiquitylation Motif: Discrepancy between HEK293 Cells and Transgenic Mice. *Int J Mol Sci* 2019;**20**.
37. Gabelli SB, Boto A, Kuhns VH, Bianchet MA, Farinelli F, Aripirala S, Yoder J, Jakoncic J, Tomaselli GF, Amzel LM. Regulation of the NaV1.5 cytoplasmic domain by calmodulin. *Nat Commun* 2014;**5**:5126.
38. Schotten U, Verheule S, Kirchhof P, Goette A. Pathophysiological mechanisms of atrial fibrillation: a translational appraisal. *Physiol Rev* 2011;**91**:265-325.
39. Nattel S, Heijman J, Zhou L, Dobrev D. Molecular Basis of Atrial Fibrillation Pathophysiology and Therapy: A Translational Perspective. *Circ Res* 2020;**127**:51-72.
40. Goette A, Kalman JM, Aguinaga L, Akar J, Cabrera JA, Chen SA, Chugh SS, Corradi D, D'Avila A, Dobrev D, Fenelon G, Gonzalez M, Hatem SN, Helm R, Hindricks G, Ho SY, Hoit B, Jalife J, Kim YH, Lip GY, Ma CS, Marcus GM, Murray K, Nogami A, Sanders P, Uribe W, Van Wagoner DR, Nattel S, Document R. EHRA/HRS/APHRS/SOLAECE expert consensus on atrial cardiomyopathies: definition, characterization, and clinical implication. *Europace* 2016;**18**:1455-1490.
41. Kirchhof PF, Fabritz CL, Franz MR. Postrepolarization refractoriness versus conduction slowing caused by class I antiarrhythmic drugs: antiarrhythmic and proarrhythmic effects. *Circulation* 1998;**97**:2567-2574.
42. Liu H, Atkins J, Kass RS. Common molecular determinants of flecainide and lidocaine block of heart Na+ channels: evidence from experiments with neutral and quaternary flecainide analogues. *J Gen Physiol* 2003;**121**:199-214.
43. Ramos E, O'Leary M E. State-dependent trapping of flecainide in the cardiac sodium channel. *J Physiol* 2004;**560**:37-49.
44. Fabritz L, Damke D, Emmerich M, Kaufmann SG, Theis K, Blana A, Fortmuller L, Laakmann S, Hermann S, Aleynichenko E, Steinfurt J, Volkery D, Riemann B, Kirchhefer U, Franz MR, Breithardt G, Carmeliet E, Schafers M, Maier SK, Carmeliet P, Kirchhof P. Autonomic modulation and antiarrhythmic therapy in a model of long QT syndrome type 3. *Cardiovasc Res* 2010;**87**:60-72.
45. Cerrone M, Remme CA, Tadros R, Bezzina CR, Delmar M. Beyond the One Gene-One Disease Paradigm: Complex Genetics and Pleiotropy in Inheritable Cardiac Disorders. *Circulation* 2019;**140**:595-610.
46. Bogeholz N, Pauls P, Kaese S, Schulte JS, Lemoine MD, Dechering DG, Frommeyer G, Goldhaber JI, Seidl MD, Kirchhefer U, Eckardt L, Muller FU, Pott C. Triggered activity in atrial myocytes is influenced by Na(+)/Ca(2+) exchanger activity in genetically altered mice. *J Mol Cell Cardiol* 2016;**101**:106-115.
47. Voigt N, Li N, Wang Q, Wang W, Trafford AW, Abu-Taha I, Sun Q, Wieland T, Ravens U, Nattel S, Wehrens XH, Dobrev D. Enhanced sarcoplasmic reticulum Ca2+ leak and increased Na+-Ca2+ exchanger function underlie delayed afterdepolarizations in patients with chronic atrial fibrillation. *Circulation* 2012;**125**:2059-2070.
48. Heijman J, Muna AP, Veleva T, Molina CE, Sutanto H, Tekook M, Wang Q, Abu-Taha IH, Gorka M, Kunzel S, El-Armouche A, Reichenspurner H, Kamler M, Nikolaev V, Ravens U, Li N, Nattel S, Wehrens XHT, Dobrev D. Atrial Myocyte NLRP3/CaMKII Nexus Forms a Substrate for Postoperative Atrial Fibrillation. *Circ Res* 2020;**127**:1036-1055.
49. Molina CE, Abu-Taha IH, Wang Q, Rosello-Diez E, Kamler M, Nattel S, Ravens U, Wehrens XHT, Hove-Madsen L, Heijman J, Dobrev D. Profibrotic, Electrical, and

Calcium-Handling Remodeling of the Atria in Heart Failure Patients With and Without Atrial Fibrillation. *Front Physiol* 2018;**9**:1383.

50. Uzun AU, Mannhardt I, Breckwoldt K, Horvath A, Johannsen SS, Hansen A, Eschenhagen T, Christ T. Ca(2+)-Currents in Human Induced Pluripotent Stem Cell-Derived Cardiomyocytes Effects of Two Different Culture Conditions. *Front Pharmacol* 2016;**7**:300.

51. Lemoine MD, Lemme M, Ulmer BM, Braren I, Krasemann S, Hansen A, Kirchhof P, Meyer C, Eschenhagen T, Christ T. Intermittent Optogenetic Tachypacing of Atrial Engineered Heart Tissue Induces Only Limited Electrical Remodelling. *J Cardiovasc Pharmacol* 2020;**77**:291-299.